MALDI Ionization Mechanisms: the Coupled Photophysical and Chemical Dynamics Model Correctly Predicts "Temperature"-Selected Spectra

Richard Knochenmuss
Switzerland

Abstract

A number of possible ultraviolet MALDI ionization mechanisms based on different fundamental phenomena have been proposed. Recently, it has been argued, based on "temperature"-selected spectra, that photoionization models should be rejected in favor of thermal ones (Ahn, et al. *J. Mass Spectrom.* **2013,** *48,* 299). Here one non-thermal photoionization model, the coupled photophysical and chemical dynamics (CPCD) model, is shown to be fully consistent with the data.

Keywords: MALDI ionization, CPCD model, DHB, photoionization, thermal ionization
rknochenmuss@gmx.net
tel: +41 33 511 1167
fax: +41 33 221 1024

Introduction

A number of different mechanisms have been proposed for MALDI ionization processes. These were reviewed relatively recently in Ref. 1. Since then, no truly new mechanisms have been proposed, but some have received renewed attention. In particular, the Kim group has recently suggested that photoionization mechanisms cannot explain a number of interesting MALDI observations.[2-6] Instead, it is suggested that MALDI ionization must be a thermal, equilibrium event.[7]

Thermal ionization in MALDI goes back at least to qualitative ideas like the polar fluid model [8, 9] and the more quantitative models of Dyer and Allwood.[10-12] The former proposes that the matrix fluid which constitutes the early plume is sufficiently solvating to allow thermal autoionization. However, it is highly unlikely that the matrix has the requisite properties, especially at plume temperatures.[1, 13] There has been some related discussion of solid state matrix properties which are relevant for this model.[14, 15] The latter, Dyer and Allwood model essentially takes the view that the MALDI plume can be treated as a hot plasma. The temperatures needed for significant ion yield in the model are at least twice the values that subsequent experiments have shown to be attained in practice.

Among non-thermal models, one that is often cited is the preformed/cluster "Lucky Survivors" model[16, 17] This proposes that all ions are formed in the preparation solution, are retained in the sample prior to laser ablation and released in the phase change process. Since, at least for some analytes, it seems to require that no reactions occur in the ablation plume,[18] this model is also not thermal. Because the final ion distribution is not proposed to reach any thermally determined equilibrium state, it appears that the proposal of Ref. [7] would reject this model.

Photoionization mechanisms may be direct or indirect. In a direct photoionization, two or more UV laser photons excite a matrix molecule or matrix aggregate (or matrix complexed

with analyte) to an ion pair state. The ionization potentials of free UV matrix molecules are too high for two photon ionization, but typical MALDI laser intensities are too low for efficient 3-photon excitation.[1] Matrix clusters have lower ionization potentials, but absorption cross sections are also very low.[19]

Certain complexes of matrix with analyte molecules have been shown to have ionization potentials in the two-photon range.[20-23] Analyte is usually present in too low concentration for this mechanism to account for the total ion yield, and total yield is not positively correlated with analyte concentration (see Rule 1 below).

Ionization involving proton transfer can require less energy than the corresponding electron transfer.[1] For some matrixes this lies in the two-photon range. However, direct photoionization by this mechanism is very unlikely since it requires excitation to a state with a different atomic configuration. As a result the Franck-Condon factors are small. An indirect variant of this is excited state proton transfer. After excitation of a molecule to a Franck-Condon accessible state, it evolves to a proton transferred state of lower energy. Neither direct nor delayed proton transfer has been observed in MALDI-relevant systems.[24]

Here we are concerned primarily with one particular non-thermal photoionization model, the coupled photophysical and chemical dynamics (CPCD) model[25-27] It invokes photoexcitation of matrix by the laser to initiate energy pooling that leads to the initial matrix ions. Photoionization is therefore indirect. These ions react with neutral analyte during the phase change and in the plume to give the final observed species. The CPCD is able to make detailed and quantitative predictions regarding numerous aspects of MALDI. This makes it possible to test the model against the observations of Ahn et al.

The key observations of the Kim group supporting the thermal proposal were summarized by them in the form of the following rules:[7]

1) For samples ablated completely, the total number of ions is independent of analyte concentration (including zero analyte concentration). An upper concentration limit for this rule was not specified, but the data reported extend up to analyte mole fractions in the high 10^{-4} range.
2) For samples ablated completely, the total number of ions is independent of laser fluence.
3) For individual laser shots, the mass spectral pattern is determined by a "temperature," which they defined by the degree of matrix fragmentation.
4) This point is not an observation, like the others, but an interpretation of observations. It is included for completeness: For individual laser shots, "the matrix-to-analyte proton transfer is in quasi-equilibrium."
5) For spectra which have been selected for their "temperature" (see 3), the spectral pattern and absolute ion abundances are independent of fluence.
6) For spectra which have been selected for their "temperature", the total number of ions is independent of the analyte and its concentration.
7) Rule 6 is valid even when more than one analyte is present.

Here these observations and the thermal hypothesis are compared to the predictions of the CPCD. In contrast to the conclusions of Ref. 7, this non-thermal photoionization model is found to be fully compatible with the data.

Methods

The coupled photophysical and chemical dynamics (CPCD) model has been described in detail elsewhere.[25-27] The model has previously not had a consistent name, being sometimes referred to as the "two-step" model. Some authors have mistakenly called it a "gas phase" model. This is incorrect, as it covers the full MALDI event, from the solid state to collision-free gas. The name introduced here is intended to reflect the fact that a range of physical and chemical processes are tightly linked in MALDI, and that a unified treatment is necessary.

Briefly, matrix ions are created by a two step exciton pooling process. Two matrix molecules

in the first laser-excited electronic state (S_1) pool their energy to give one highly excited matrix molecule (S_n state), and a ground state molecule. $S_n + S_1$ or S_n pooling is also included, to concentrate sufficient energy on one molecule to ionize it. Radiative and non-radiative decay processes are included. Matrix parameters are based on experimental data for DHB.

The sample is assumed to ablate at a fixed temperature (450 K), and then to expand isentropically. The ablated material is assumed to completely vaporize. All bimolecular reaction rates are scaled by the collision rate change after ablation. Here, a 0.1 mm laser spot is assumed to be uniformly illuminated by a 355 nm Nd:YAG laser beam, with 5 ns halfwidth gaussian temporal profile. Laser propagation into the sample is included, both absorption and stimulated emission.

The calculation can be carried out for only the top layer of a sample, or integrated over the full ablated depth. The former is believed to correspond to many experimental measurements, since few mass spectrometers can efficiently collect and focus ions generated over the wide velocity and density regimes found in the early MALDI plume. A similar conclusion was reached by Soltwisch et al. in a recent study of several MALDI matrixes.[28]

Depth integration is carried out by dividing the sample into slices of varying depth. Since the laser is attenuated exponentially with depth, the thicknesses are adjusted for equal laser energy absorption. Surface layers are therefore thinner than deep layers.The model is numerically integrated for each layer and the results summed. The number of layers is increased until no change in the results is observed. A typical number of layers is 150, as used here.

The material expands supersonically, and top layers ablate both earlier and faster than deeper layers.[29] Mixing and energy exchange are therefore negligible between layers in the plume. The expansion velocity includes an offset due to thermal expansion prior to phase

change.

Analyte ions are formed by charge transfer reaction with the primary matrix ions. The kinetic equations use Arrhenius rates to model the ion-molecule reactions. The necessary activation energies are obtained from non-linear free energy relationships as a function of reaction exoergicity. Parameters for protonation / deprotonation reactions were assumed in this work, which is appropriate for a large range of MALDI applications. Other charge transfer reactions, of electrons, cations or anions can also be modeled.

In Ref. [7], most measurements were made using fairly basic peptides as analytes, such as Y_5K or Y_5R. Unless noted otherwise, in the calculations reported here, the analyte (or analytes) was assumed to have MW=950 Da. Unless otherwise noted, the proton transfer reaction free energy from protonated matrix to analyte was taken to be -150 kJ/mol. The transfer from protonated analyte to matrix was -50 kJ/mol. The matrix parameters were for DHB.

Ion yields are shown in the subsequent figures as mole fractions of the total population. All species sum at all times to a total of 1. Charge and mass balance were checked during the integration, which used double precision, 5^{th} order Runge-Kutta methods, with adaptive step size, and a truncation relative error limit of $<=10^{-8}$, in the Igor Pro environment (Wavemetrics, Lake Oswego, Oregon, USA). An example calculation is shown in Fig. 1, along with the resulting calculated positive and negative mass spectra.

Figure 1 here

Results and Discussion

Consider first Rule 1: for full ablation, ion yield is independent of analyte concentration. Full ablation was defined as ablation down to the substrate. As far as the CPCD model is concerned, full ablation is the sum of all layers which receive enough laser energy to undergo phase change. At a constant fluence, this depth is fixed, so we can assume the sample to

have that thickness. The quantity to calculate is the depth-integrated ion yield as a function of analyte concentration. This result is shown in Fig. 2.

Figure 2 here

Over the range of concentrations used in Ref. 7, and at a constant laser fluence of twice the ablation threshold, the total (matrix + analyte) CPCD yield is indeed independent of analyte concentration. This is true not only for analytes of a given molecular weight, but also if they are of different molecular weight. This demonstrates that the CPCD is consistent with the observations underlying Rule 1.

Figure 2 also shows that Rule 1 is not expected to hold at higher analyte concentrations. In the CPCD all primary ions are matrix ions. Reducing the matrix concentration by adding analyte reduces the number of primary ions which can be created in a particular volume. Since secondary analyte ions are derived from primary matrix ions, the total yield must drop. In this high concentration region, matrix and analyte suppression effects also become very significant, and relative spectral intensities are a poor reflection of original sample composition.

Figure 2 was calculated assuming that the analytes do not absorb the laser, and are inert in primary ionization processes. This is the expected behavior for many analytes, including the peptides tested in Ref. 7. However, it is possible for analytes to interfere with primary ionization. This was demonstrated by Setz and Knochenmuss, with a laser dye that can act as a trap for matrix excitons.[30] This analyte was able to significantly reduce yields even at mole fractions in the low 10^{-8} range. A modified version of the CPCD including trapping was shown to reproduce the concentration dependence of the ion yield over 3 orders of magnitude. Rule 1 therefore applies only to inert analytes. This revision and the observations behind it also are arguments against the thermal hypothesis. If ionization is always thermal, it should not matter if an analyte can act as a trap for matrix excitations.

Rule 2 states that the full-ablation yield is constant regardless of fluence. Figure 3 shows total CPCD ion yields vs. fluence, both raw and normalized to the ablated depth. The depth-normalized values were then scaled to correspond to the depth ablated by the highest fluence event, to facilitate comparison with Rule 2.

Figure 3 here

The unscaled yield increases linearly with fluence, not with a higher order, even though the energy needed to create an ion pair corresponds to more than one photon. During the dense period of plume expansion, the recombination rate will increase proportionately to the concentration of each ion species, so approximate cancellation of formation and loss is expected. It is the race between recombination and physical expansion which determines how much or little of the original ions remain to be detected. Due to this compensation, the net fluence dependence not as strong as might be expected from consideration of ion formation processes alone.

The dashed line, yield normalized for ablation depth, is nearly flat over the fluence range of Ref. 7, with a slight downward trend. This result is consistent with the observations underlying Rule 2. Certain known effects are not included here. Experimentally, the sample is found to be modified by the first shots, and yields per shot decrease with shot number,[31-35] These would cause the dashed line to drop toward lower fluence, where more shots are required to fully ablate a given sample depth.

The CPCD prediction is that Rule 2, like Rule 1, is not universally applicable, but will become less valid at lower fluences, for DHB matrix. The high fluence plateau is consistent with measurements of Soltwisch et al.[28, 36] For other matrixes, the yield goes through a broad maximum at mid fluences, then drops at high fluences.[28, 36] The CPCD also reproduces this effect, as will be shown in a forthcoming publication.

Rule 3 is that the spectral pattern is determined by the "temperature" in the early plume, defined this using the degree of matrix fragmentation. Under the assumption that this is a unimolecular, effectively irreversible, activated process, such a measure might indeed be indicative of the highest temperatures experienced by matrix molecules. Unimolecular dissociation of well-characterized "thermometer" analytes has previously been used to characterize MALDI plumes in this way.[37]

However, it does not follow that all reactions are characterized by the same peak temperature. Reactions that are reversible under plume conditions will not reflect a peak temperature, but will be determined by integration over the full MALDI event, especially the later, cooler plume. Reactions that fall in this category are cation-anion recombination, and proton (or other charge carrier) transfer reactions. These are the important MALDI bimolecular reactions.

Rule 3 can therefore only be valid for thermal models if charge transfer and neutralization reactions are only reversible at the peak MALDI temperature, and frozen after that. Otherwise, as the plume expands and cools, the ion yield would decrease dramatically. The CPCD does not include this assumption. The extent of charge transfer reactions in the CPCD depends on the amount of primary ions and the rate at which the plume expands (modulating bimolecular reaction rates). Both of these are determined by the laser fluence and sample absorption cross section. Since the peak temperature reached is also determined by the same parameters, it is evident that the spectral pattern will be the same for the same fluence. It can be concluded that the CPCD predicts the data underlying Rule 3, but does not support the implicit freezing interpretation.

The observation underlying Rule 4, "the matrix-to-analyte proton transfer is in quasi-equilibrium," is that matrix/analyte ion ratios do not vary much in selected spectra, for the tested analytes, concentrations and fluences. Similar to Rule 3, it does not follow from the

observations that equilibrium is required, nor that the pattern is determined by the peak temperature reflected by unimolecular decays.

Departure from equilibrium is particularly evident in the ratio of positive to negative analyte ions in MALDI. For a given analyte, the ratio varies little with matrix-analyte charge transfer free energy, although it should change significantly if it is in equilibrium.[38] CPCD calculations showed that the data are consistent with kinetically limited reverse reactions, if the forward matrix-to-analyte reaction has a significant driving force in at least one polarity.[27]

Rule 5 is: for spectra which have been selected for their "temperature", the spectral pattern and absolute ion abundances are independent of the fluence. For the CPCD, Rule 5 is effectively the same as Rule 3. Selecting spectra to have the same "temperature" is equivalent to selecting layers of the sample that have absorbed an identical amount of laser energy per unit volume. Figure 4 illustrates this.

Figure 4 here

The depth-integrated CPCD proceeds by summation of sequentially calculated layers of increasing depth below the surface. The top layer experiences the highest laser fluence, and absorbs some of the laser energy. The layer below it therefore experiences a lower fluence, and so on. Because higher layers absorb more energy per unit volume, they are hotter, ablate earlier and expand faster. There is therefore little or no mass or energy exchange between layers. Plotting the ion yields as a function not of depth, but of fluence incident on each layer, as in Fig. 4, shows how there are always layers of identical fluence and identical ion yields, for any total incident fluence. The vertical line at a layer fluence of 20 mJ/cm^2 illustrates this in the figure. For all three incident fluences, there is a layer which experiences 20 mJ/cm^2 fluence, and this layer always produces the same amount of matrix and analyte ions.

Rules 6 and 7 say that for spectra which have been selected for their "temperature" (a

specified layer fluence in the CPCD), the total number of ions is independent of the analytes and their concentration. A CPCD result illustrating consistency with this rule is shown in Figure 5. The concentration range investigated in Ref. 7 is in the left corner of the plot, marked by heavy lines. In this region, and beyond, the total ion current remains virtually unchanged, for a layer of constant fluence.

Figure 5 here

The surface in this region is flat because, at a fixed fluence, the number of primary ions does not change. Also the plume expands the same regardless of analyte amount, so losses are constant. However, as shown in Fig. 2, at higher analyte concentrations primary ion production is degraded so the surface of Fig. 5 droops toward the right corner. In other words, the CPCD predicts that Rules 6 and 7 have limited ranges of applicability, similar to the limits of Rule 1.

The CPCD can also be used to further examine "temperature" selected MALDI and to compare it with conventional MALDI. Figure 6 shows the ratio of positive analyte ion signals (A1/A2) over a range of analyte concentrations. This is more interesting than total ion yield because matrix yield is usually irrelevant to the analytical problem. In Fig. 6 The ion signal ratios are normalized by the initial concentration ratio in the sample. Ideally, this normalized ratio would be constant and equal to unity. Then relative concentrations in the original sample could be derived directly from the relative spectral intensities.

Figure 6 here

In both the constant fluence and depth-integrated results of Fig. 6 there is a central plateau where the spectral ratios correctly reflect the sample concentrations (log(ion ratio)=0). As the concentration imbalance becomes more pronounced, the MALDI spectra become less reliable guides to the sample composition. The more abundant analyte is overrepresented. Of course at higher analyte concentrations, the Analyte Suppression Effect[39] becomes even more

pronounced, potentially leading to complete loss of signal of one of the analytes.

The deviations from ideality are largest at low fluences. This reflects competition between analytes for the less abundant primary matrix ions. The "temperature" selected (single layer) and conventional surfaces are nearly identical near the MALDI threshold, there is no analytical advantage to either method. At high fluence, around 3 times the threshold, the selected surface is somewhat flatter than the conventional one. However, the latter assumes that all ablated layers can be equally efficiently sampled by the mass spectrometer. If there is a velocity window or other bias, the spectra will be selected in that way, flattening the surface.

Figure 6 was calculated for identical charge transfer reaction free energies for both analytes. This is the most favorable situation for measuring relative analyte concentrations by MALDI, but it is not typical. If the charge transfer energetics are very different for the two analytes, the surfaces might be as in Fig. 7.

Figure 7 here

In spite of unequal reaction free energies, the surfaces in Fig. 7 are very similar to those of Fig. 6. There is a small vertical offset, but otherwise no qualitative difference. This suggests that the selected spectra method does not offer any fundamental benefit in relative quantitation over conventional MALDI. It is fundamentally a form of selection based on spectral quality indicators, a technique which is used in several forms already.

Conclusions

One non-thermal photoionization model, the CPCD, has been shown to be compatible with the empirical MALDI rules recently proposed in Ref. 7. The key advantages of the CPCD in this context are the coupling of reaction rates to the plume expansion, and its explicit treatment of reaction rates throughout the MALDI event. Assumptions regarding reaction equilibria and reaction freezing are not required. Other models may or may not also be compatible with the rules, the objective of this work is simply to show that the CPCD is compatible with the data. The CPCD also predicts there are limits on the ranges and conditions of validity of the rules.

The relative performance of "temperature" selected MALDI compared to conventional methods were investigated as a function of analyte concentrations, fluence and charge transfer energetics. At high fluence, the selected spectra may have some advantages for quantitation, but the difference is not expected to be large. The main advantage of selected spectra in practice may be in reduction of signal variability.

References

[1] R. Knochenmuss. Ion formation mechanisms in UV-MALDI. *The Analyst* **2006,** *131,* 966.

[2] Y. J. Bae, J. H. Moon, M. S. Kim. Expansion Cooling in the Matrix Plume is Under-Recognized in MALDI Mass Spectrometry. *J. Am. Soc. Mass Spectrom.* **2011,** *22,* 1070.

[3] Y. J. Bae, K. M. Park, M. S. Kim. Reproducibility of Temperature-Selected Mass Spectra in Mastrix-Assisted Laser Desorption Ionization of Peptides. *Anal. Chem.* **2012,** *84,* 7107.

[4] Y. J. Bae, Y. S. Shin, J. H. Moon, M. S. Kim. Degree of Ionization in MALDI of Peptides: Thermal Explanation for the Gas-Phase Ion Formation. *J. Am. Soc. Mass Spectrom.* **2012,** *23,* 1326.

[5] J. H. Moon, Y. S. Shin, Y. J. Bae, M. S. Kim. Ion Yields for Some Salts in MALDI: Mechanism for the Gas-Phase Ion Formation from Preformed Ions. *J. Am. Soc. Mass Spectrom.* **2011,** *23,* 162.

[6] J. H. Moon, S. H. Yoon, M. S. Kim. Temperature of Peptide Ions Generated by Matrix-Assisted Laser Desorption Ionization and Their Dissociation Kinetic Parameters. *J. Phys. Chem. B* **2009,** *113,* 2071.

[7] S. H. Ahn, K. M. Park, Y. J. Bae, M. S. Kim. Quantitative reproducibility of mass spectra in matrix-assisted laser desorption ionization and unraveling of the mechanism for gas-phase peptide ion formation. *J. Mass Spectrom.* **2013,** *48,* 299.

[8] X. Chen, J. A. Carroll, R. C. Beavis. Near-Ultraviolet-Induced Matrix-Assisted Laser Desorption/Ionization as a Function of Wavelength. *J. Am. Soc. Mass Spectrom.* **1998,** *9,* 885.

[9] S. Niu, W. Zhang, B. T. Chait. Direct Comparison of Infrared and Ultraviolet Wavelength Matrix-Assisted Laser Desorption/Ionization Mass Spectrometry of Proteins. *J. Am. Soc. Mass Spectrom.* **1998,** *9,* 1.

[10] D. A. Allwood, R. W. Dreyfus, I. K. Perera, P. E. Dyer. UV Optical-Absorption of Matrices Used for Matrix-Assisted Laser Desorption/Ionization. *Rapid Commun. Mass Spectrom.* **1996,** *10,* 1575.

[11] D. A. Allwood, P. E. Dyer, R. W. Dreyfus. Ionization Modeling of Matrix Molecules in Ultraviolet Matrix-Assisted Laser Desorption/Ionization. *Rapid Commun. Mass Spectrom.* **1997,** *11,* 499.

[12] D. A. Allwood, P. E. Dyer, R. W. Dreyfus, I. K. Perera. Plasma Modeling of Matrix-Assisted UV Laser-Desorption/Ionization (MALDI). *Appl. Surf. Sci.* **1997,** *110,* 616.

[13] R. Knochenmuss. MALDI and Related Methods: A Solved Problem or Still a Mystery? *Mass Spectrom. (Japan)* **2013,** 22*,* S0006.

[14] Y.-H. Lai, C.-C. Wang, S.-H. Lin, Y. T. Lee, Y.-S. Wang. Solid-Phase Thermodynamic Interpretation of Ion Desorption in Matrix-Assisted Laser Desorption/Ionization. *J. Phys. Chem. B* **2010,** *114,* 13847.

[15] Y.-H. Lai, C.-C. Wang, C. W. Chen, B.-H. Liu, S. H. Lin, Y. T. Lee. Analysis of Initial Reactions of MALDI Based on Chemical Properties of Matrixes and Excitation Condition. *J. Phys. Chem. B* **2012,** *116,* 9635.

[16] M. Karas, R. Krueger. Ion Formation in MALDI: the cluster ionization mechanism. *Chem. Rev.* **2003,** *103,* 427.

[17] M. Karas, M. Glückmann, J. Schäfer. Ionization in MALDI: singly charged molecular ions are the lucky survivors. *J. Mass Spectrom.* **2000,** *35,* 1.

[18] T. W. Jaskolla, M. Karas. Compelling Evidence for Lucky Survivor and Gas Phase Protonation: The Unified MALDI Analyte Protonation Mechanism. *J. Am. Soc. Mass Spectrom.* **2011,** *22,* 976.

[19] Q. Lin, R. Knochenmuss. Two-photon ionization thresholds of matrix-assisted laser desorption/ionization matrix clusters. *Rapid Comm. Mass Spectrom.* **2001,** *15,* 1422.

[20] C. M. Land, G. R. Kinsel. Investigation of the Mechanism of Intracluster Proton Transfer from Sinapinic Acid to Biomolecular Analytes. *J. Am. Soc. Mass Spectrom.* **1998,** *9,* 1060.

[21] C. M. Land, G. R. Kinsel. The mechanism of matrix to analyte proton transfer in clusters of 2,5 dihydroxybenzoic acid and the tripeptide VPL. *J. Am. Soc. Mass Spectrom.* **2001,** *12,* 726.

[22] G. Kinsel, R. Knochenmuss, P. Setz, C. M. Land, S.-K. Goh, E. F. Archibong, J. H. Hardesty, D. Marynick. Ionization energy reductions in small 2,5-dihydroxybenzoic acid-proline clusters. *J. Mass Spectrom.* **2002,** *37,* 1131.

[23] G. R. Kinsel, Q. Zhao, J. Narayanasamy, F. Yassin, H. V. Rasika Dias, B. Niesner, K. Prater, C. St. Marie, L. Ly, D. Marynik. Arginine/2,5-dihydroxybenzoic acid clusters: an

experimental and theoretical study of the gas-phase and solid-state systems. *J. Phys. Chem. A* **2004,** *108,* 3153.

[24] V. Karbach, R. Knochenmuss. Do Single Matrix Molecules Generate Primary Ions in Ultraviolet Matrix-Assisted Laser Desorption/Ionization? *Rapid Commun. Mass Spectrom.* **1998,** *12,* 968.

[25] R. Knochenmuss. A Quantitative Model of Ultraviolet Matrix-assisted Laser Desorption and Ionization. *J. Mass Spectrom.* **2002,** *37,* 867.

[26] R. Knochenmuss. A Quantitative Model of UV-MALDI Including Analyte Ion Generation. *Anal. Chem.* **2003,** *75,* 2199.

[27] R. Knochenmuss. A bipolar rate equation model of MALDI primary and secondary ionization processes, with application to positive/negative analyte ion rations and suppression effects. *Int. J. Mass Spectrom.* **2009,** *285,* 105.

[28] J. Soltwisch, T. W. Jaskolla, F. Hillenkamp, M. Karas, K. Dreisewerd. Ion Yields in UV-MALDI Mass Spectrometry As a Function of Excitation Laser Wavelength and Optical and Physico-Chemical Properties of Classical and Halogen Substituted MALDI Matrixes. *Anal. Chem.* **2012,** *84,* 6567.

[29] R. Knochenmuss, L. V. Zhigilei. Molecular dynamics simulations of MALDI: laser fluence and pulse width dependence of plume characteristics and consequences for matrix and analyte ionization. *J. Mass Spectrom.* **2010,** *45,* 333.

[30] P. Setz, R. Knochenmuss. Exciton Mobility and Trapping in a UV-MALDI Matrix. *J. Phys. Chem. A* **2005,** *109,* 4030.

[31] M. Sadeghi, A. Vertes. Crystallite Size Dependence of Volatilization in Matrix-Assisted Laser Desorption Ionization. *Appl. Surf. Sci.* **1998,** *127/129,* 226.

[32] I. Fournier, C. Marinach, J.-C. Tabet, G. Bolbach. Irradiation effects in MALDI, ablation, ion production and surface modifications. Part II: 2,5-dihydroxybenzoic acid monocrystals. *J. Am. Soc. Mass Spectrom.* **2003,** *14,* 893.

[33] I. Fournier, J.-C. Tabet, G. Bolbach. Irradiation effects in MALDI and surface modifications Part I: Sinapinic acid monocrystals. *Int. J. Mass Spectrom.* **2002,** *219,* 515.

[34] R. Knochenmuss, G. McCombie, M. Faderl. The dependence of MALDI ion yield on metal substrates: photoelectrons from the metal vs. surface-enhanced matrix photoionization. *J. Phys. Chem. A* **2006,** *110,* 12728.

[35] G. McCombie, R. Knochenmuss. Enhanced MALDI ionization efficiency at the metal-matrix interface: practical and mechanistic consequences of sample thickness and preparation method. *J.Am. Soc. Mass Spectrom.* **2006,** *17,* 737.

[36] J. Soltwisch, T. W. Jaskolla, K. Dreisewerd. Color Matters – Material Ejection and Ion Yields in UV-MALDI Mass Spectrometry As a Function of Laser Wavelength and Laser Fluence. *Submitted* **2013.**

[37] G. Luo, I. Marginean, A. Vertes. Internal energy of ions generated by MALDI. *Anal. Chem.* **2002,** *74,* 6185.

[38] M. Dashtiev, E. Wäfler, U. Röhling, M. Gorshkov, F. Hillenkamp, R. Zenobi. Positive and negative analyte ion yield in matrix-assisted laser desorption/ionization. *Int. J. Mass Spectrom.* **2007,** *268,* 122.

[39] R. Knochenmuss, A. Stortelder, K. Breuker, R. Zenobi. Secondary ion-molecule reactions in MALDI. *J. Mass Spectrom.* **2000,** *35,* 1237.

Figures

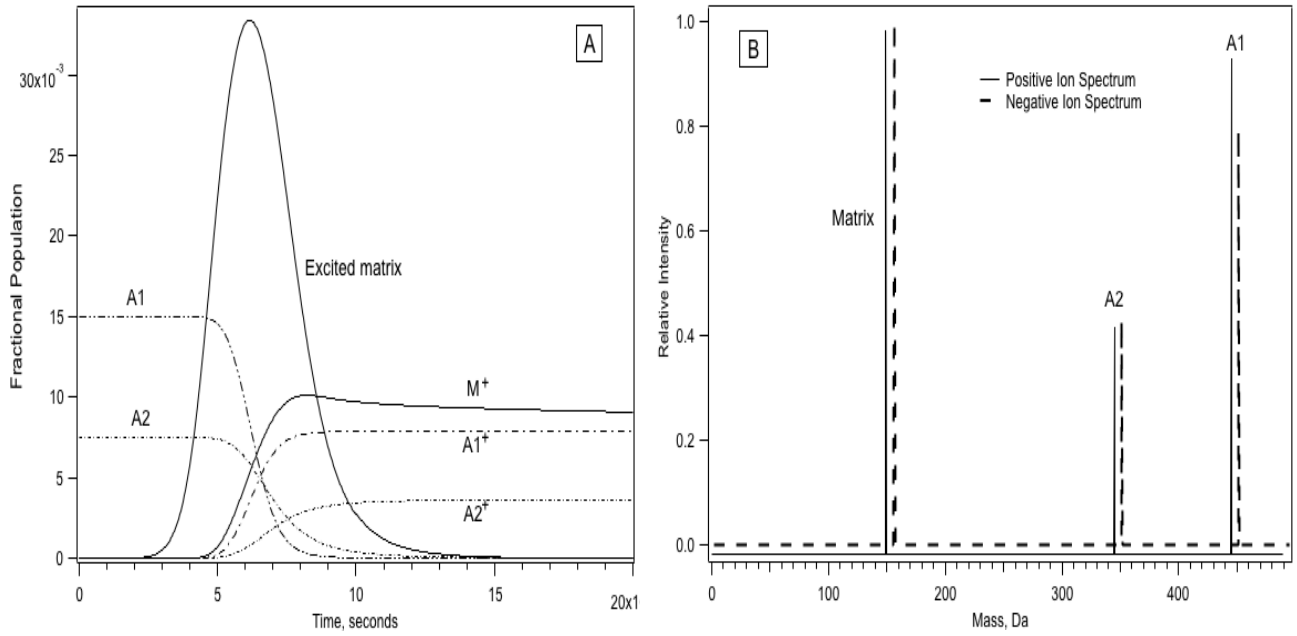

Figure 1. Panel A is an example of the time evolution of some of the species included in the CPCD model. For simplicity, only the two analytes, excited DHB matrix and positive ions are shown. Panel B shows the resulting ion abundances in both positive and negative modes at 200 ns, normalized to the largest peak in each case. The negative ion spectrum is offset for clarity The laser fluence was 17 mJ/cm$^{2.}$ The analyte parameters were A: 0.015 0.mole fraction, ΔG=-150 kJ/mol for charge transfer from matrix positive ions, ΔG=-50 kJ/mol for charge transfer from matrix positive ions. B: 0.0075 0.mole fraction, ΔG=-75 kJ/mol for charge transfer from matrix positive ions, ΔG=-75 kJ/mol for charge transfer from matrix positive ions.

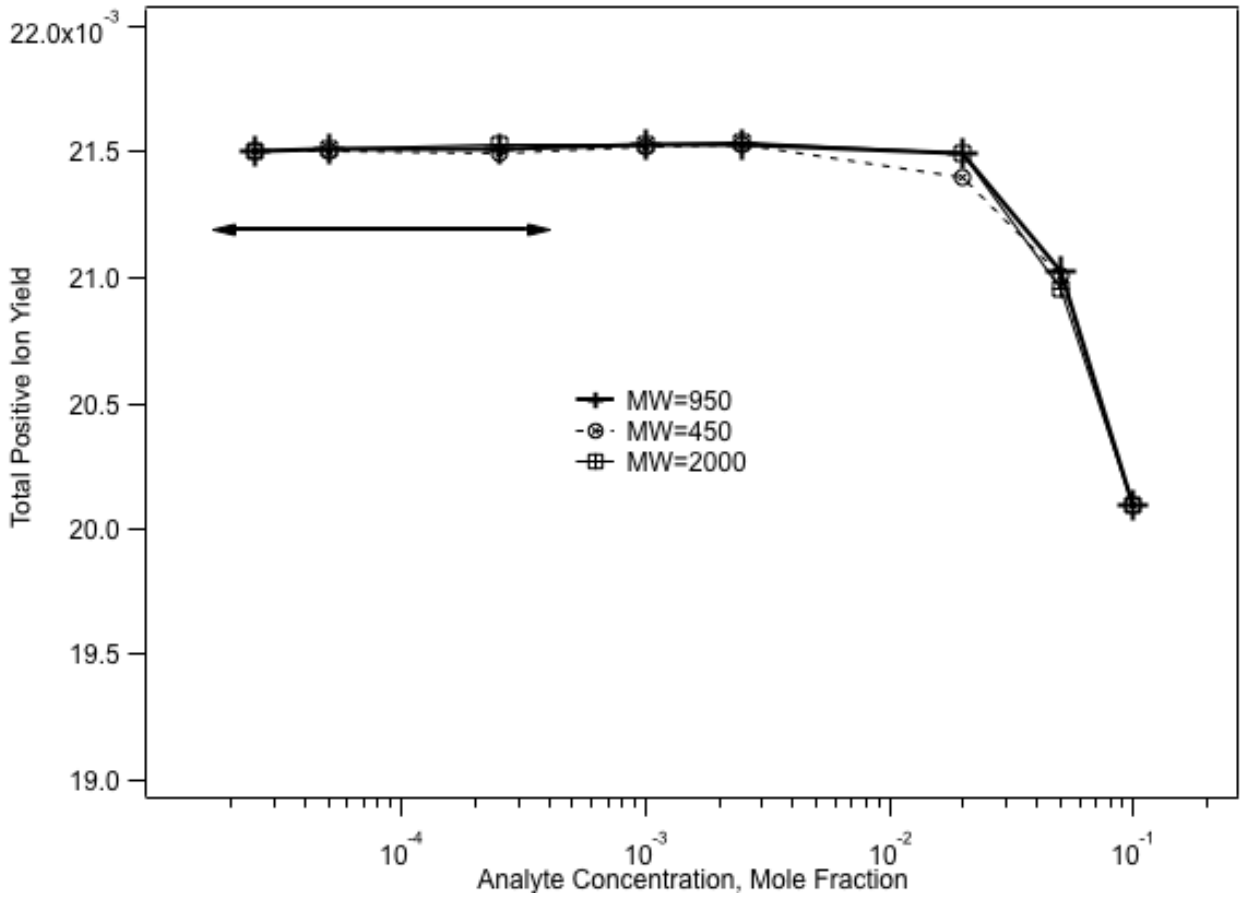

Figure 2. Calculated total (matrix plus analyte) positive ion yield over a range of analyte mole fractions in the sample. The laser fluence was 24 mJ/cm^2, about twice the threshold. The yield was summed over the full ablated depth. The concentration range tested in Ref. [7] is indicated by the double arrow. There is no analyte concentration dependence of the total ion yield in this range, demonstrating CPCD consistency with the with data underlying Rule 1. As shown, the rule could also be extended to state that there no molecular weight effect. At higher concentrations the CPCD predicts the rule will not hold.

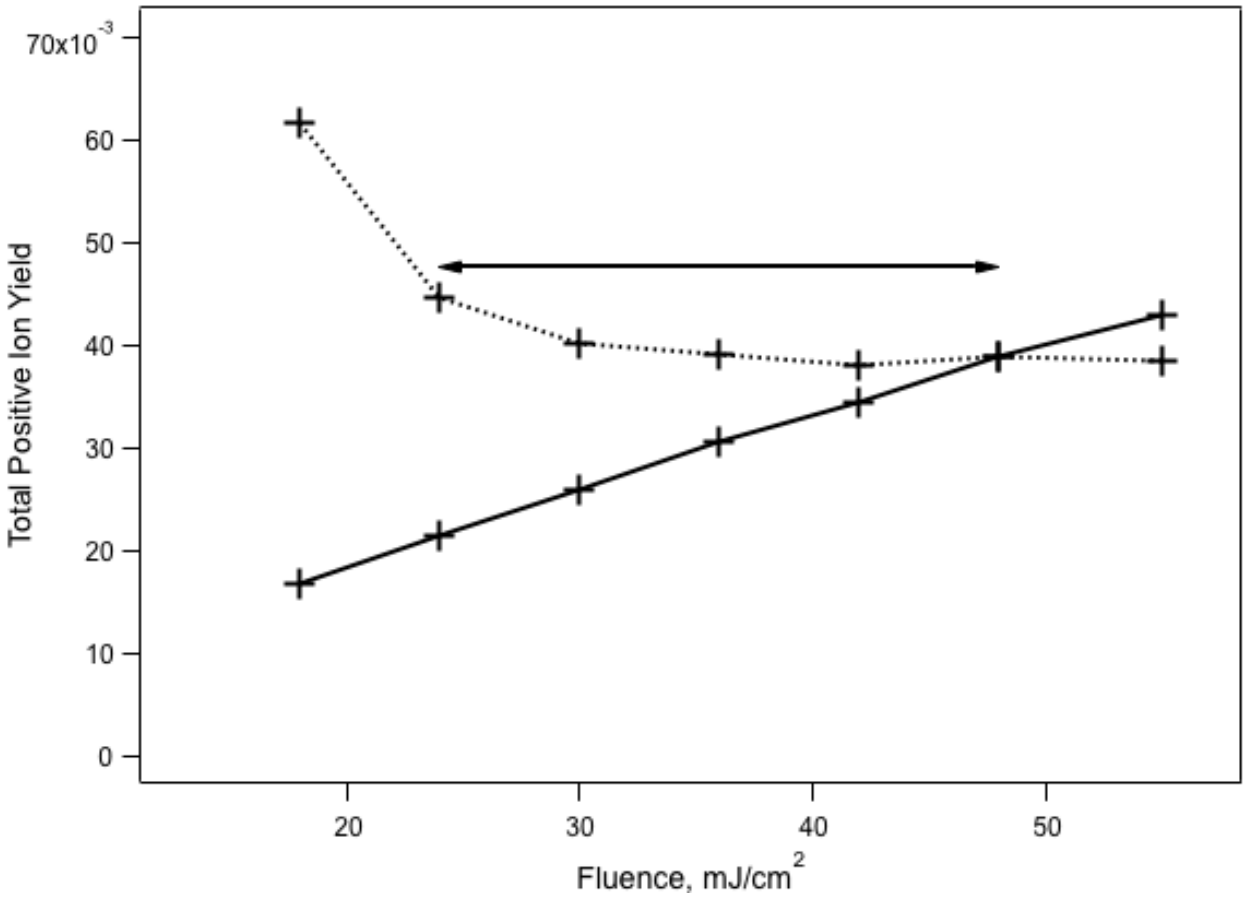

Figure 3. Calculated total (matrix plus analyte) positive ion yield versus fluence, at an analyte mole fraction of 1.2 x 10^{-4}. The solid line is the unscaled ion yield. Since more material is ablated at higher fluences, the lower fluence points must be scaled to reflect the condition of Rule 2, that the same depth of material is ablated. This depth-normalized curve is shown as a dashed line. The fluence range corresponding to that tested in Ref. 7 (2-4 times the threshold) is indicated by the double arrow. The flat or slightly decreasing trend in this region is consistent with the data underlying the rule.

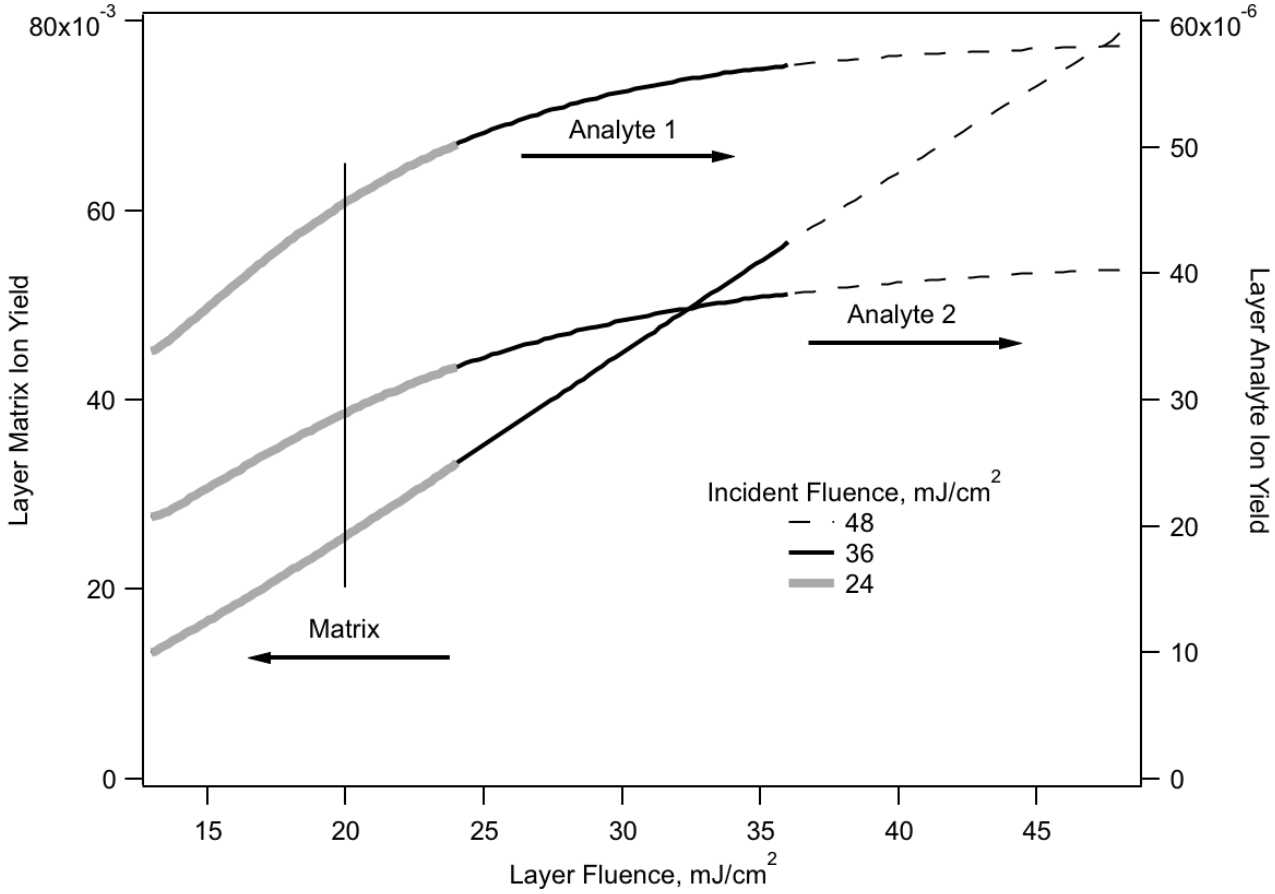

Figure 4. Calculated matrix and analyte positive ion yields versus layer in the sample, for three impinging fluences. The mole fraction of analyte 1 was 1.2 x 10^{-4}, and that of analyte 2 was 9 x 10^{-5}. Rather than layer depth, the horizontal axis is the fluence each layer experienced, due to attenuation by overlying layers. The top layer of each sample experienced the nominal impinging fluence, 24, 36 or 48 mJ/cm^2. The deepest layers which were ablated received about 12 mJ/cm^2. The vertical line at 20 mJ/cm^2 illustrates that each sample contained a layer which experienced this fluence. Spectra selected to reflect this fluence, for example by using patterns of matrix ions, give identical quantities of analyte ions. This demonstrates the consistency of the CPCD with Rule 5.

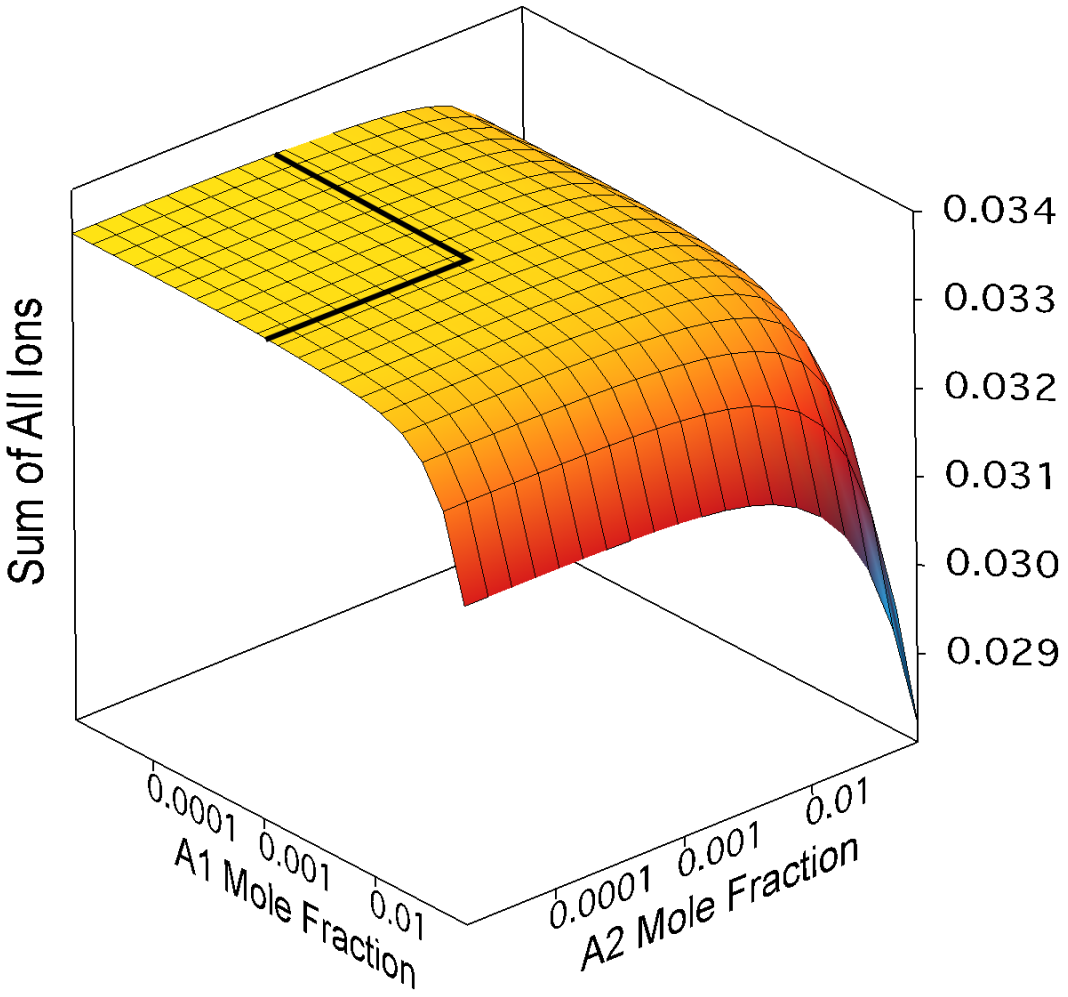

Figure 5. Calculated single layer total positive ion yield (mole fraction) at a fluence of 30 mJ/cm^2, for a range of initial concentrations of two analytes. The charge transfer free energies from matrix to analyte were for both analytes: ΔG(positive) = -150 kJ/mol and ΔG(negative) = -75 kJ/mol. The concentration range investigated in Ref. 7 is to the left of the region marked by heavy lines.

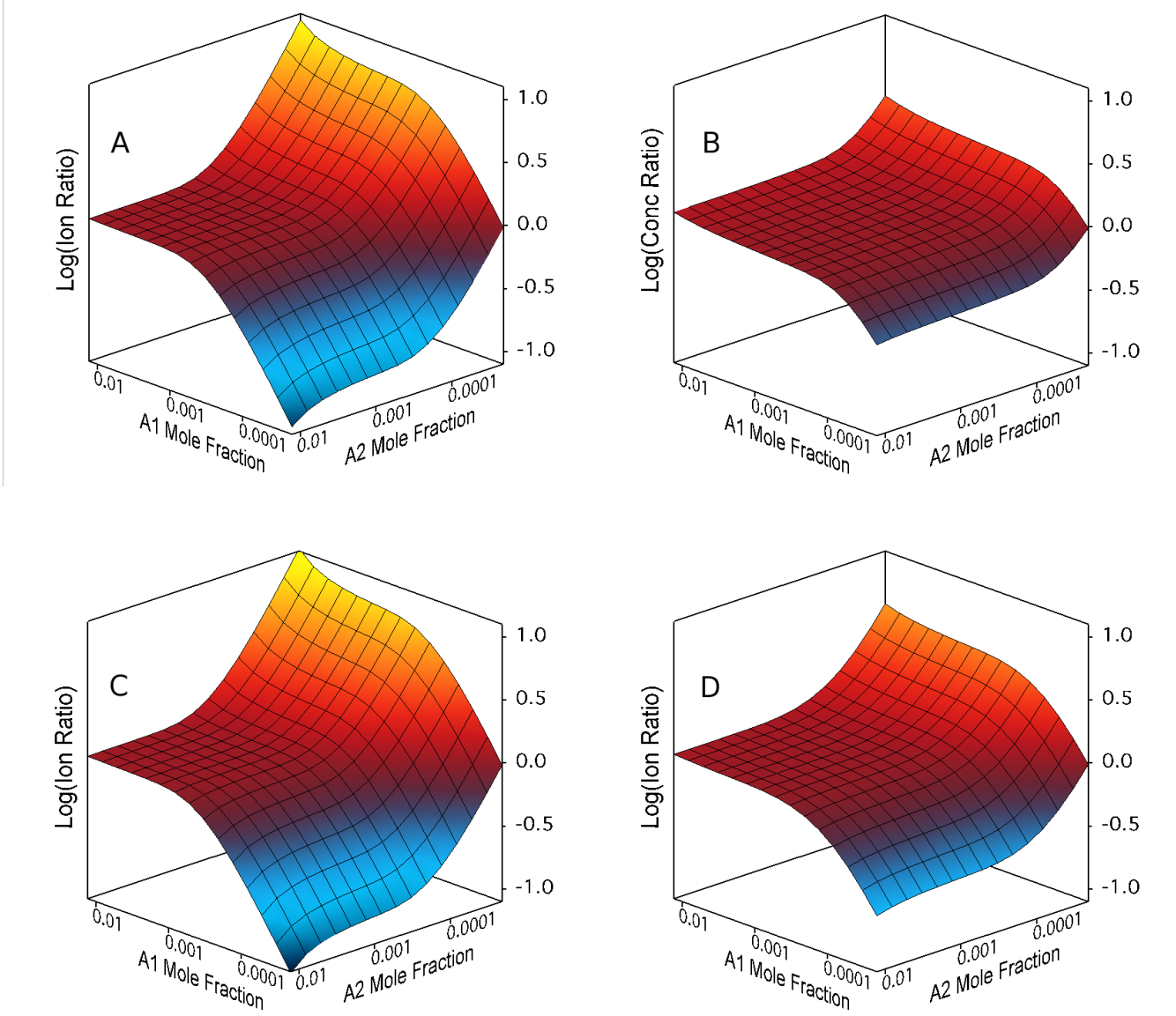

Figure 6. Normalized ratios of two positive analyte ions, over a range of analyte concentrations. The analytes reacted equally strongly with the matrix primary ions (ΔG = -150 kJ/mol). The data are divided by the concentration ratio in the sample, so a ratio of 0=log(1) means the mass spectrum exactly reflects the initial concentrations ((analyte 1 ions/analyte 2 ions) / (analyte 1 concentration / analyte 2 concentration)). The upper two panels are for selected sample layers receiving 15 (A) and 45 mJ/cm^2 (B). This corresponds

to "temperature" selected spectra. The bottom two panels are fully depth integrated, corresponding to a conventional MALDI experiment, with the same incident fluences, 15 (C) and 45 mJ/cm^2 (D). The low fluence surfaces are nearly identical. At high fluence, the single layer ("selected" MALDI) surface is flatter, so this method may have some utility for relative quantitation under these conditions.

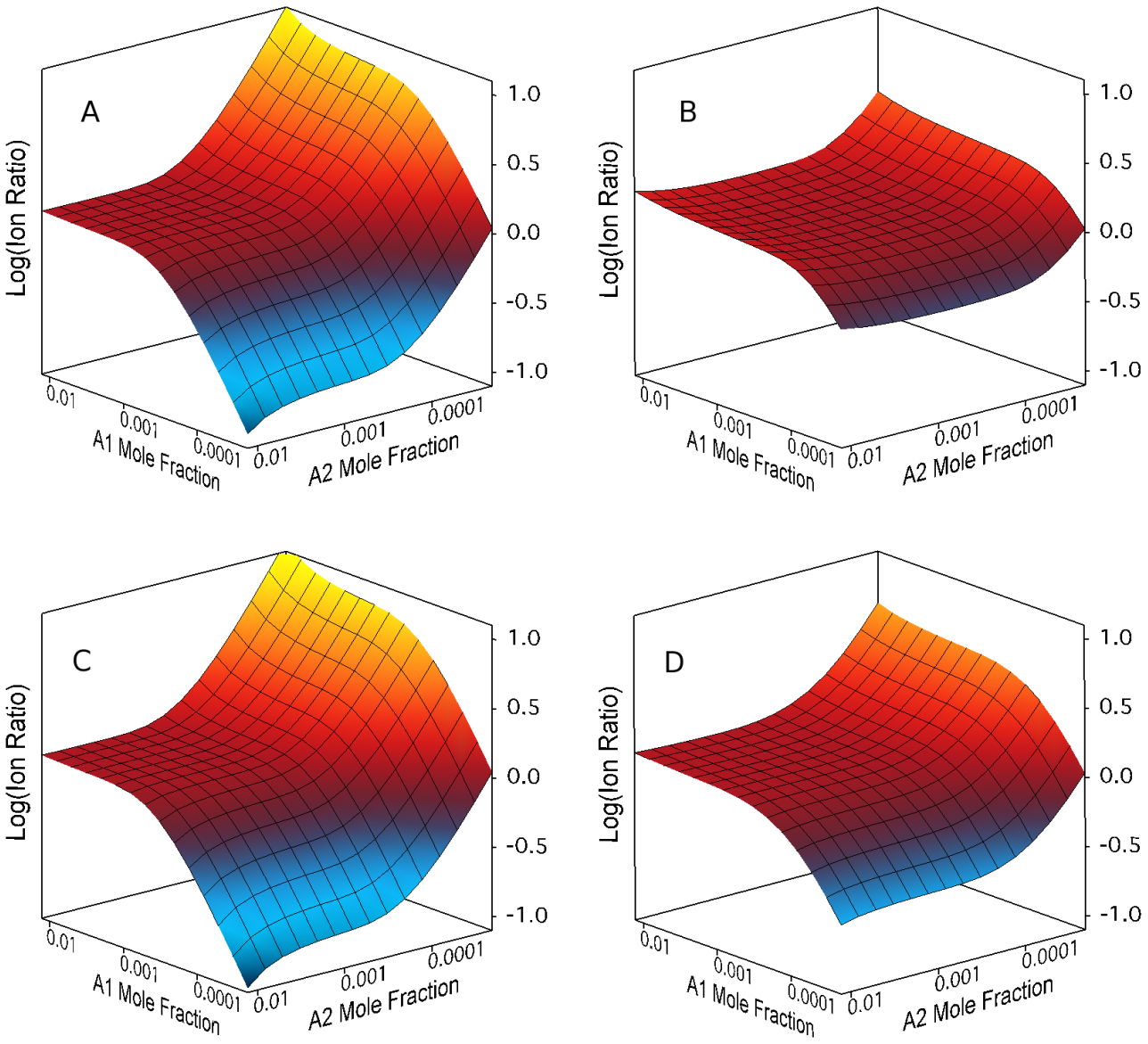

Figure 7. Normalized positive ion ratios as in Figure 5, but the matrix-analyte reaction energetics were not identical for the two analytes. Reaction of analyte 1 was taken to have a ΔG of -150 kJ/mol, while that of analyte 2 was -50 kJ/ mol. In the opposite polarity, the deprotonation reactions were taken to have the inverse values (-50 and -150 kJ/mol). The upper panels A and B are represent single sample layers ("selected" MALDI), while the lower two are depth integrated. Left fluences are 15 and right are 45 mJ/cm^2.